CSIRO PUBLISHING

Full Paper

www.publish.csiro.au/journals/ajc

Aust. J. Chem. **2011**, *64*, 345–354

Crystal Structures, Antioxidation, and DNA Binding Properties of Sm^{III} Complexes

Yongchun Liu,[A,B] *Zhengyin Yang,*[A,C] *Kejun Zhang,*[B] *Yun Wu,*[B] *Jihua Zhu,*[B] *and Tianlin Zhou*[B]

[A]College of Chemistry and Chemical Engineering, State Key Laboratory of Applied Organic Chemistry, Lanzhou University, 730000 Lanzhou, China.

[B]College of Chemistry and Chemical Engineering, Key Laboratory of Longdong Biological Resources in Gansu Province, Longdong University, 745000 Qingyang, Gansu, China.

[C]Corresponding author. Email: yangzy@lzu.edu.cn

The dinuclear Sm^{III} complexes with 1:1 metal to ligand stoichiometry were prepared from $Sm(NO_3)_3 \cdot 6H_2O$ and three anionic tetradentate Schiff-base ligands derived from 8-hydroxyquinoline-2-carboxyaldehyde with benzoylhydrazine, 2-hydroxybenzoylhydrazine, and isonicotinylhydrazine, respectively. All the ligands and complexes can bind strongly to calf thymus DNA through intercalation with the binding constants at 10^5–$10^6\,M^{-1}$, but complexes present stronger affinities to DNA than ligands. All the ligands and complexes have strong abilities of antioxidation, but complexes and ligands containing an active phenolic hydroxy group show stronger scavenging effects on hydroxyl radical, and Sm^{III} complex containing *N*-heteroaromatic substituent shows stronger scavenging effects for superoxide radical.

Manuscript received: 12 August 2010.
Manuscript accepted: 7 February 2011.

Introduction

The chemistry of quinoline and its derivatives have attracted special interest due to their therapeutic properties. Quinoline sulfonamides have been used in the treatment of cancer, tuberculosis, diabetes, malaria, and convulsion.[1] Apart from the magnetic and photophysical properties, the bioactivities of lanthanides such as antimicrobe, antitumour, antivirus, anticoagulant action, enhancing natural killer and macrophage cell activities, prevention from arteriosclerosis, etc., have also been paid attention in recent decades.[2] In addition, Schiff bases are able to inhibit the growth of several animal tumours, and some metal chelates also have shown good antitumour activities against animal tumours.[3] So, well designed organic ligands enable a fine tuning of special properties of the metal ions.

DNA is an important cellular receptor, and many chemicals exert their antitumour effects through binding to DNA thereby changing the replication of DNA and inhibiting the growth of the tumour cells. This is the basis of designing new and more efficient antitumour drugs and their effectiveness depends on the mode and affinity of the binding.[4] Several metal chelates, as agents for mediation of strand scission of duplex DNA and as chemotherapeutic agents, have been used as probes of DNA structure in solution.[5] Moreover, AT-rich sequences are believed to favour metal complex binding at the minor groove when the handedness of the complex is complementary to that of the right-handed helix of DNA.[6]

However, an excess of activated oxygen species in the forms of superoxide anion ($O_2^{\bullet-}$) and hydroxyl radical ($OH^{\bullet}$), generated by normal metabolic processes, may cause various diseases such as carcinogenesis, drug-associated toxicity, inflammation, atherogenesis, and aging in aerobic organisms.[7] The potential value of antioxidants has prompted investigators to search for the cooperative effects of metal complexes and natural compounds for improving antioxidant activity and cytotoxicity.[8] It has been recently demonstrated that some minor groove binders for DNA are effective inhibitors of the formation of a DNA/tumour-associated transplantation antigen(-box-)-binding protein (TBP) complex or topoisomerases. Adding a reactive entity endowed with oxidative properties should improve the efficiency of inhibitors.[9]

Previously, the antioxidation and DNA binding properties of Eu^{III} complexes derived from these ligands were investigated.[10] In this paper, the Sm^{III} complexes were investigated as the same methods. Furthermore, the substituent effects of these compounds on antioxidation and DNA binding properties were investigated further.

Results and Discussion

Synthesis of Ligands and Sm^{III} Complexes

Three Schiff-base ligands, 8-hydroxyquinoline-2-carboxyaldehyde-(benzoyl)hydrazone (**1a**, H_2L^1), 8-hydroxyquinoline-2-carboxyaldehyde-(salicyloyl)hydrazone (**1b**, H_2L^2), and 8-hydroxyquinoline-2-carboxyaldehyde-(isonicotinyl)hydrazone (**1c**, H_2L^3) were prepared from equimolar amounts of 8-hydroxyquinoline-2-carboxyaldehyde and benzoylhydrazine, 2-hydroxybenzoylhydrazine and isonicotinylhydrazine as the literature, respectively.[10] The synthetic routes for ligands are presented in Scheme 1, then their powdered Sm^{III} complexes

© CSIRO 2011
10.1071/CH10302 0004-9425/11/030345

(**2a**, **2b**, and **2c**) were easily prepared from the corresponding ligands and equimolar amounts of $Sm(NO_3)_3 \cdot 6H_2O$. All the Sm^{III} complexes are of orange powders, stable in air, and soluble in DMF and DMSO, but slightly soluble in methanol, ethanol, acetonitrile, ethyl acetate, acetone, THF, and $CHCl_3$. The melting points of all of the Sm^{III} complexes exceed 300°C.

Crystal Structure Analyses of the Sm^{III} Complexes

The orange transparent, X-ray quality crystals of **2a′**, **2b′**, and **2c′** were obtained by vapour diffusion of diethyl ether into DMF solution of the metal complexes (recrystallization in DMF suitable for X-ray measurements) at room temperature for 2 weeks. Crystal data and structure refinements for the X-ray structural analyses, selected bond lengths, and angles of the Sm^{III} complexes are presented in Tables 1, 2, and Accessory Publication.

The coordination sphere of *ORTEP* diagrams (30% probability ellipsoids) in Fig. 1a and b shows that the compositions of **2a′** and **2b′** are of $[SmL^1(NO_3)(DMF)_2]_2$ and $[SmL^2(NO_3)(DMF)_2]_2$, respectively. Either of **1a** and **1b** acts as a dibasic tetradentate, binding to Sm^{III} through the phenolate oxygen atom, the nitrogen atom of quinolinato unit, the C=N group,

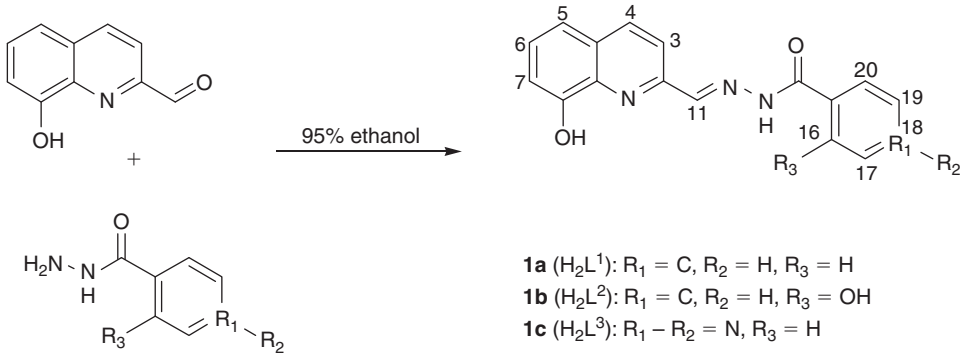

Scheme 1. The synthetic routes for ligands.

Table 1. Crystal data and structure refinement for the metal complexes

Complex	$[SmL^1(NO_3)(DMF)_2]_2$ (**2a′**)	$[SmL^2(NO_3)(DMF)_2]_2$ (**2b′**)	$2[SmL^3(NO_3)(DMF)_2]_2 \cdot 5DMF$ (**2c′**)
CCDC deposition number	704943	704944	704945
Chemical formula	$C_{46}H_{50}N_{12}O_{14}Sm_2$	$C_{46}H_{50}N_{12}O_{16}Sm_2$	$C_{103}H_{131}N_{33}O_{33}Sm_4$
Formula weight	1295.68	1327.70	2960.81
T [K]	294(2)	294(2)	294(2)
Wavelength [Å]	0.71073	0.71073	0.71073
Radiation	Mo-Kα	Mo-Kα	Mo-Kα
Crystal system	Monoclinic	Monoclinic	Triclinic
Space group	$P2_1/c$	$P2_1/c$	$P\bar{1}$
a [Å]	11.3808(10)	11.5812(8)	12.5913(7)
b [Å]	18.755(2)	18.1196(13)	14.7267(8)
c [Å]	12.4846(12)	12.8473(10)	17.9592(9)
α [°]	90.00	90.00	90.4910(10)
β [°]	93.216(2)	95.6680(10)	90.9250(10)
γ [°]	90.00	90.00	100.3210(10)
V [Å^3]	2660.6(5)	2682.8(3)	3275.6(3)
Z	2	2	1
D_c [g cm^{-3}]	1.617	1.646	1.501
μ [mm^{-1}]	2.259	2.245	1.850
$F(000)$	1292	1328	1492
Crystal size [mm]	0.37 × 0.18 × 0.08	0.15 × 0.12 × 0.10	0.30 × 0.28 × 0.25
$\theta_{min/max}$ [°]	1.79–25.01	1.77–28.85	1.64–25.50
Index ranges	$-13 \le h \le 13$, $-22 \le k \le 20$, $-13 \le l \le 14$	$-15 \le h \le 12$, $-20 \le k \le 24$, $-15 \le l \le 16$	$-14 \le h \le 15$, $-17 \le k \le 16$, $-21 \le l \le 16$
Reflections collected	13176	16632	17264
Independent reflections	4661 ($R_{int} = 0.1095$)	6649 ($R_{int} = 0.0355$)	12067 ($R_{int} = 0.0169$)
Absorption correction	Semi-empirical from equivalents	Semi-empirical from equivalents	Semi-empirical from equivalents
Max. and min. transmission	0.8400 and 0.4887	0.7993 and 0.7314	0.6549 and 0.6069
Refinement method	Full-matrix least-squares on F^2	Full-matrix least-squares on F^2	Full-matrix least-squares on F^2
Data/restraints/parameters	4661/0/338	6649/0/308	12067/0/839
Goodness-of-fit on F^2	1.088	0.977	1.024
Final R indices [$I > 2\sigma(I)$]	$R_1 = 0.0669$, $wR_2 = 0.1228$	$R_1 = 0.0386$, $wR_2 = 0.0756$	$R_1 = 0.0393$, $wR_2 = 0.1057$
R indices (all data)	$R_1 = 0.1434$, $wR_2 = 0.1521$	$R_1 = 0.0686$, $wR_2 = 0.0855$	$R_1 = 0.0555$, $wR_2 = 0.1176$
$\rho_{min/max}$ [e Å^{-3}]	1.479/–0.922	0.942/–0.632	0.666/–0.967

and the $^{-}$O–C=N– group (enolized and deprotonated from O=C–NH–) of the aroylhydrazone side chain, where the bond lengths of $^{-}$O–C and N=C of **2a′** are 1.289(13) and 1.339(14) Å, respectively, while 1.280(5) and 1.332(6) Å for **2b′**. In addition, one DMF molecule is binding orthogonally to the ligand-plane from one side to the metal ion, while another DMF and a nitrate (bidentate) are binding from the other. Dimerization of this monomeric unit occurs through the phenolate oxygen atoms leading to a central four-membered $(SmO)_2$-ring with the Sm···Sm separation of 4.0713(12) Å for **2a′** and 4.0599(5) Å for **2b′**. At the dimerization site, the 'set off' of the two SmL^1-planes by 1.702 Å takes place and of the two SmL^2-planes by 1.766 Å. However, the 2-hydroxyl substituent of **2b′** may form an intra-molecular hydrogen bond with the adjacent nitrogen atom (1.839 Å) of the same side chain.

The crystal structure of a dimolecule and dinuclear 2 $[SmL^3(NO_3)(DMF)_2]_2\cdot 5DMF$ complex (**2c′**) with a 1:1 metal to ligand and nine-coordination is shown in Fig. 1c. Dimerization of the monomeric unit of one molecule occurs through the phenolate oxygen atoms leading to a central four-membered $(SmO)_2$-ring with the Sm(1)···Sm(1)#1 separation of 4.0291(5) Å and another with the Sm(2)···Sm(2)#2 separation of 4.0171(5) Å. At the dimerization sites, the 'set off' of the two 'Sm(1)L^3-planes' by 1.748 Å takes place and of the two 'Sm(2) L^3-planes' by 1.733 Å. Moreover, in one molecule (Sm(1)) of the independent crystal cell, the O=C–NH– group of the isonicotinylhydrazine side chain has enolized and deprotonated into $^{-}$O–C=N– with the bond lengths of 1.277(7) and 1.320(8) Å for $^{-}$O–C and N=C, respectively, while in another molecule (Sm(2)), 1.286(6), and 1.309(7) Å for $^{-}$O–C and N=C, respectively. In addition, there are five free DMF solvent molecules in the lattice of **2c′**, however, parts of them are disordered.

Structure Analyses of the Powdered Sm^{III} Complexes

Elemental Analysis and Molar Conductance

Elemental analyses indicate that all the powdered Sm^{III} complexes are of 1:1 metal to ligand (stoichiometry) complexes. The data of molar conductance of the Sm^{III} complexes in DMF solutions indicate that they all act as non-electrolytes.[11]

Infrared Spectrum Study of the Powdered Complexes

The characteristic IR spectrum band [ν_{max}/cm^{-1}] data of the powdered Sm^{III} complexes are listed in Table S2. Carefully compared with the characteristic IR bands of ligands, it comes to the conclusion that: (1) $3429–3399_{br}\,cm^{-1}$ assigned to ν(OH) of H_2O, $947–935_w\,cm^{-1}$ assigned to ρ_r (H_2O) and $656–639_w\,cm^{-1}$ assigned to ρ_w (H_2O) indicate coordinated water molecules participating in the Sm^{III} complexes;[12] (2) $1100–1102\,cm^{-1}$ assigned to ν(C–OM) indicate the binding of metal ion to ligand through an O–M linkage;[13] (3) $1682–1643_s\,cm^{-1}$ assigned to ν(CO) and $3576–3359_v\,cm^{-1}$ assigned to ν(NH) of ligands disappeared in all the IR spectra of Sm^{III} complexes, indicating that they participate in the Sm^{III} complexes; (4) 1635–$1601\,cm^{-1}$ assigned to ν(CN) of azomethines of the Sm^{III} complexes, shifting by 22–6 cm^{-1} in comparison with bands of ligands, indicate the nitrogen atoms of azomethines participating in the complexes; $1565–1548\,cm^{-1}$ assigned to ν(CN) of pyridines of the Sm^{III} complexes, shifting by 9–16 cm^{-1}, indicate the nitrogen atoms of pyridines also participating in the complexes. However, the band of $1591\,cm^{-1}$ can be assigned to ν(CN) of free pyridine of isonicotinylhydrazine side chain; (5) $535–521_w\,cm^{-1}$ assigned to ν(MO) and $488–486_w\,cm^{-1}$ assigned to ν(MN) further indicate that oxygen atom and nitrogen atom participate in Sm^{III} complexes; (6) all the Sm^{III} complexes show 1498–1492 (ν_1), 1316–1311 (ν_4), 1061–1034 (ν_2), 839–811 (ν_3), 765–756 (ν_5), and 184–178 (ν_1–ν_4) cm^{-1}, indicating that nitrate ions bidentately participate in the Sm^{III} complexes.[10]

Additionally, the ESI-MS data show that the *m/z* ($[M+H]^+$, DMF solution) are 1297.1, 1329.2, and 1299.2 for dinuclear complexes **2a′**, **2b′**, and **2c′**, respectively, indicating that the four-coordinated water molecules can be replaced by four DMF molecules when the powdered Sm^{III} complexes are dissolved in DMF solution. Furthermore, the *m/z* data ($[M/2+H]^+$, DMF solution), 648.2, 665.4, and 649.2, can also be found for **2a′**, **2b′**,

Table 2. Important bond lengths and angles of 2a′, 2b′, and 2c′ (Sm1) complexes

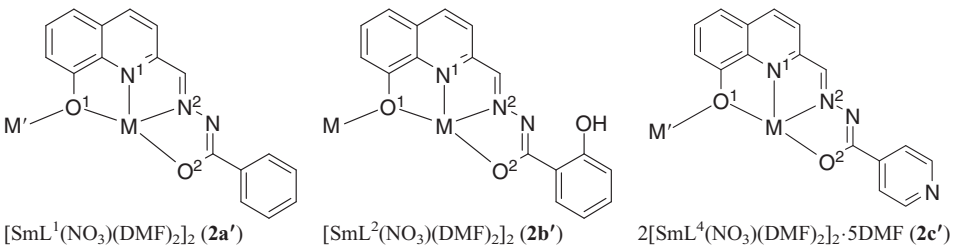

	$[SmL^1(NO_3)(DMF)_2]_2$ (**2a′**)	$[SmL^2(NO_3)(DMF)_2]_2$ (**2b′**)	$2[SmL^4(NO_3)(DMF)_2]_2\cdot 5DMF$ (**2c′**)
O1–M	2.462(7)	2.445(3)	2.441(4)
N1–M	2.545(8)	2.522(3)	2.544(4)
N2–M	2.591(9)	2.582(3)	2.562(5)
O2–M	2.374(8)	2.382(3)	2.377(4)
O1–M′	2.420(7)	2.426(3)	2.423(4)
O1–M–N1	65.0(3)	65.11(10)	64.76(14)
N1–M–N2	61.6(3)	61.35(12)	61.87(16)
N2–M–O2	61.5(3)	61.34(11)	62.00(15)
Distance between the parallel ML-planes	1.702	1.766	1.748
Distance between M···M′	4.0713(12)	4.0599(5)	4.0291(5)

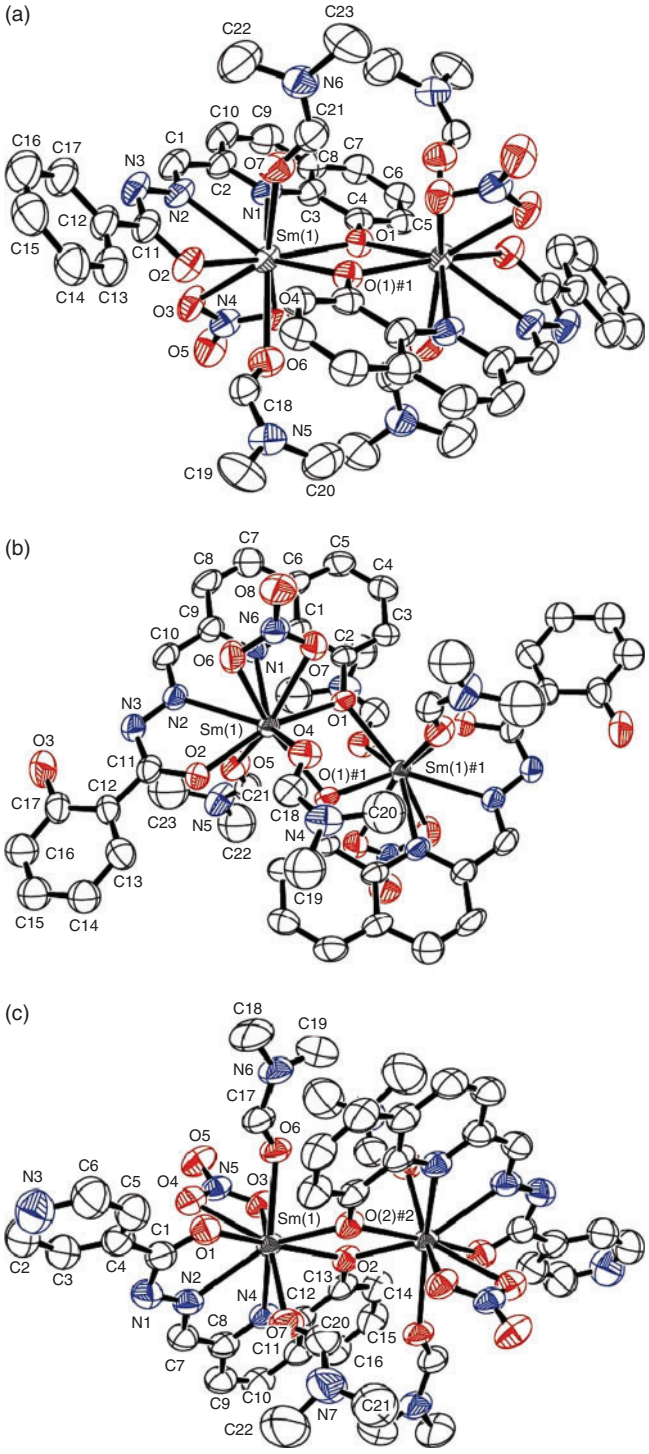

Fig. 1. Coordination spheres of *ORTEP* diagrams of (a) $[SmL^1(NO_3)(DMF)_2]_2$, (b) $[SmL^2(NO_3)(DMF)_2]_2$, and (c) $2[SmL^3(NO_3)(DMF)_2]_2 \cdot 5DMF$ complexes.

and **2c′**, respectively, indicating that there exists monomeric unit in DMF solution. In summary, the results of elemental analyses, molar conductance, IR and ESI-MS data indicate that all of the powdered metal complexes are structurally similar to each other and the compositions are of $[SmL^{1-3}(NO_3)(H_2O)_2]_2$, which slightly differ from their crystal structures. Furthermore, compared with the spectrum of free ligand, the ^{1}H NMR spectra of complexes widen and shift to a certain extent (Fig. S1), indicating that complexes have paramagnetism or single electrons in their molecular orbits, so the complexes do not have an S=0 ground state though they are dinuclear.

DNA Binding Properties

Viscosity Titration Measurements

Viscosity measurements are very sensitive to changes in the length of DNA, as viscosity is proportional to L^3 for rod-like DNA of length L. Viscosity titration measurements were carried out to clarify the interaction mode between the investigated compounds and CT-DNA. The effects of ligands and Sm^{III} complexes on the viscosities of CT-DNA are shown in Fig. S2. With the ratios of the investigated compounds to DNA increasing, the relative viscosities of DNA increase steadily, indicating that there exists intercalation between all the ligands and Sm^{III} complexes with the DNA helix.[14,15] In addition, the relative viscosities of DNA increase with the order of **1a** > **1b** > **1c**, the order of **2a** > **2b** > **2c** and the orders of **1b** > **1a**, **2b** > **2a**, **2c** > **1c**. These suggest the extents of the unwinding and lengthening of the DNA helix by compounds and the affinities of compounds binding to DNA, which may be due to the key roles of substituent effects and the larger coplanar structures of Sm^{III} complexes than those of ligands. Intercalation has been traditionally associated with molecules containing fused bi/tricyclic ring structures, although atypical intercalators with non-fused rings systems may be more prevalent than previously recognized.[16] So it is logical that all the large coplanar Sm^{III} complexes containing fused multiple cyclic ring structures and ligands containing fused bicyclic ring structures can bind to DNA through intercalation.

Ultraviolet-visible (UV-vis) Spectroscopy Study

The UV-vis spectra values of the maximum absorption wavelength (λ_{max}), the molar absorptivity (ε), and the hypochromicity at λ_{max} for ligands and Sm^{III} complexes are listed in Table S3. The UV-vis spectra of ligands show two types of absorption bands at λ_{max} in the regions of 290–295 ($\varepsilon = 2.86$–$3.55 \times 10^4\ M^{-1}\ cm^{-1}$) and 323–329 nm ($\varepsilon = 1.78$–$2.36 \times 10^4\ M^{-1}\ cm^{-1}$), which can be assigned to π–π* transition within the organic molecules. The UV-vis spectra of Sm^{III} complexes, however, show two types of absorption bands at λ_{max} in the regions of 323–327 ($\varepsilon = 3.66$–$4.39 \times 10^4\ M^{-1}\ cm^{-1}$) and 371–378 nm ($\varepsilon = 2.75$–$3.60 \times 10^4\ M^{-1}\ cm^{-1}$), which can be respectively assigned to π–π* transition of the larger conjugated organic molecules and π–π* of the C=N–N=C groups coupled with charge transfer from ligand to metal ion ($L \rightarrow Sm^{3+}$).[12] The band shift of λ_{max} and the change of ε for complex in comparison with ligand indicate the formation of the Sm^{III} complex.

Upon successive addition of CT-DNA, the UV-vis absorption bands of **1a**, **1b**, and **1c** show a progressive hypochromism of 34.3% at 295 nm, 30.1% at 294 nm, and 8.4% at 290 nm by approximately saturated titration end points with C_{DNA}:C_{ligand} = 1.4–2.0:1, with 1, 3, and 0 nm red shifts respectively, of absorption bands in the region of 290–295 nm. **1a**, **1b**, and **1c** show another progressive hypochromism of 11.1% at 323 nm, 18.1% at 329 nm, and 1.0% at 325 nm, respectively, with 1, 3, and 0 nm blue shifts in the region of 323–329 nm. Similarly, upon successive addition of CT-DNA, the UV-vis absorption bands of **2a** and **2b** show a progressive hypochromism of 24.9% at 324 nm and 20.6% at 323 nm by approximately saturated titration end points at C_{DNA}:$C_{complex}$ = 1.4–1.6:1, with 1 and 2 nm red shifts respectively, of absorption bands. However, **2c**

show a slightly unsteady hypochromism of 0.54% at 327 nm and no band shift in the region of 323–327 nm by the saturated titration end point at C_{DNA}:$C_{complex}$ = 1.6:1. **2a**, **2b**, and **2c** show another progressive hypochromism of 22.3% at 371 nm, 21.5% at 378 nm, and 0.94% at 374 nm, respectively, but all of them show no band shift in the region of 371–378 nm. In addition, isosbestic points at 327–343 nm for ligands and 408–422 nm for Sm^{III} complexes are observed, indicating that a reaction equilibrium between every investigated compound and DNA takes place.

Absorption titration can monitor the interaction of a compound with DNA. The obvious hypochromism and red shift are usually characterized by the non-covalently intercalative binding of a compound to DNA helix, due to the strong stacking interaction between the aromatic chromophore of the compound and base pairs of DNA.[17] Some studies have revealed that hypochromism and no band shift or small red shifts at λ_{max} are in keeping with groove binding.[18] In order to clarify whether hypochromism and the red shift of the absorption band can be used as positive criterions for DNA binding mode, UV-vis titration experiments of ethidium bromide (EB)-DNA system were performed by the same methods as these investigated compounds. The UV-vis titration spectra of EB-DNA system and the plot of A/A_o versus C_{DNA}/C_{EB} at 285 nm (λ_{max}) are shown in Fig. S3. Upon successive addition of CT-DNA, the absorption bands of EB (classical intercalator) at 285 nm show a progressive hypochromism that can be divided into two regions by a turning titration ratio of $C_{DNA(nucleotides)}$:C_{EB} at 4.5:1 or an inverse ratio of C_{EB}:C_{DNA} at 0.22:1, which exactly represents the maximum number of EB bound per nucleotide of DNA.[19] Starting with successive addition of CT-DNA to the turning titration ratio, the UV-vis absorption band of EB at 285 nm shows a progressive hypochromism of 34.2% with only a 1 nm red shift. But hereafter, red shifts of 6 nm take place with the total hypochromism of 47.7% by approximately the titration end point at C_{DNA}:C_{EB} = 10.4:1. It is difficult for most intercalators, especially the moderates, to reach such an isobath of absorption bands as EB. In fact, some groove binders of Hoechst 33258 family can also present red shifts or even blue shifts of absorption bands when they bind to a DNA helix by groove binding modes, especially for multiple binders.[20] Therefore, the intercalation between a compound and DNA cannot be excluded only by no or small red shift of UV-vis absorption band. After all, hydrodynamic measurements that are sensitive to length change of DNA (i.e. viscosity and sedimentation) are regarded as the least ambiguous and the most critical criterions for binding modes in solution in absence of crystallographic structural data.[21]

However, the magnitude of hypochromism is parallel to the intercalative strength and the affinity of a compound binding to DNA.[22] The appreciable hypochromisms of ligands and Sm^{III} complexes intercalating to DNA present the order of **1a** > **1b** > **1c** and **2a** > **2b** > **2c**, which are in good agreement with the viscosity titration results. Here, the effect of substituent may play key roles in the interaction. Besides the same structural units of these Sm^{III} complexes, as for **2a**, the phenyl substituent may be more accessible to DNA helix and much more favourable of forming π–π stacking interaction between the aromatic chromophore of the complex and the base pairs of DNA than **2b**. In the latter, the 2-hydroxy locating in benzoylhydrazine side chain may induce some non-negligible steric hindrances when intercalating into the DNA helix. As for **2c**, the N atom of aromatic sextet of the pyridine ring of isonicotinylhydrazine side chain has an exposed and non-hybridized p orbit containing long pair electrons, which may result in a stronger electronic repulsion and hinder the π–π stacking interaction. Moreover, the aggregation of self-stacked molecules of **2c** may occur, which will induce the possibilities of an association-dissociation equilibrium in the absence of DNA, and induce a slightly unsteady UV-vis absorption and a little hypochromism even in an excess of conjugate versus DNA bps.[20b] For the same reasons, the hypochromicity for ligands shows the same order as the Sm^{III} complexes.

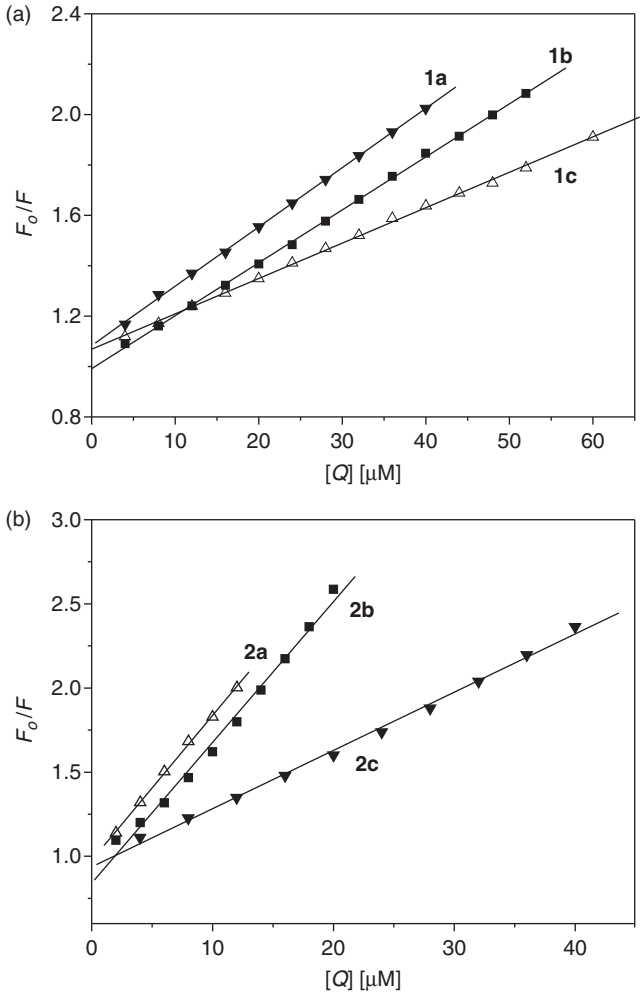

Fig. 2. Stern–Volmer plots of F_o/F versus [Q] for (a) ligands and (b) Sm^{III} complexes.

EB-DNA Quenching Assay

The EB-DNA quenching tests were performed and quantified by fluorescent titration. The fluorescence emission intensity of EB-DNA system decreased dramatically upon the increasing amounts of every ligand and Sm^{III} complex. The Stern–Volmer equation was used to determine the fluorescent quenching mechanism.[14a] Plots of F_o/F versus [Q] are shown in Fig. 2 and the quenching data collected and calculated from the good linear relationship when $P < 0.05$ are listed in Table 3. As shown, the data of K_{SV} are 1.405–2.352 × 10^4 M^{-1} for ligands and 3.463–8.596 × 10^4 M^{-1} for Sm^{III} complexes, accordingly, the data of K_q calculated are 0.7806–1.307 × 10^{13} M^{-1} s^{-1} for ligands and 1.924–4.776 × 10^{13} M^{-1} s^{-1} for Sm^{III} complexes, in which the value of τ_o is taken as 1.8 × 10^{-9} s.[14a] All of the current values of K_q are much greater than that of $K_{q(max)}$ (2.0 × 10^{10} M^{-1} s^{-1}),

Table 3. Parameters of K_b, K_{SV}, K_q, CF_{50}, IC_{50} ($OH^{\bullet}$ and $O_2^{-\bullet}$) for ligands and the Sm^{III} complexes
R represents the linear correlation coefficient

Compound	$K_b \times 10^5\ M^{-1}$	$1/n$[A]	$K_{SV} \times 10^4\ M^{-1}$ [*R*]	$K_q \times 10^{13}\ M^{-1}\ s^{-1}$	FC_{50}[B] $\times 10^{-5}$ M ($C_{compound}/C_{DNA,\ nucleotides}$)	SC_{50}[C] [μM] for $OH^{\bullet}$ [*R*]	SC_{50}[C] [μM] for $O_2^{-\bullet}$ [*R*]
1a	2.148 ± 0.205	0.081	2.086 ± 0.014 (0.9997)	1.169	4.818 (12.05)	14.66 ± 0.495 (0.9937)	6.831 ± 0.219 (0.9954)
1b	9.295 ± 1.315	0.28	2.352 ± 0.018 (0.9998)	1.307	3.895 (9.738)	7.716 ± 0.230 (0.9940)	4.308 ± 0.174 (0.9892)
1c	1.329 ± 0.180	0.092	1.405 ± 0.013 (0.9995)	0.7806	6.630 (16.58)	76.10 ± 0.372 (0.9909)	5.131 ± 0.258 (0.9838)
2a	10.91 ± 1.690	0.14	8.358 ± 0.289 (0.9953)	4.643	1.386 (3.465)	3.792 ± 0.145 (0.9662)	2.696 ± 0.079 (0.9906)
2b	37.32 ± 6.440	0.20	8.596 ± 0.151 (0.9994)	4.776	1.189 (2.973)	2.127 ± 0.046 (0.9862)	5.678 ± 0.153 (0.9958)
2c	2.562 ± 0.310	0.12	3.463 ± 0.076 (0.9981)	1.924	3.072 (7.680)	2.194 ± 0.044 (0.9884)	1.727 ± 0.025 (0.9934)

[A]The data of $1/n$ represent moles of the tested compound bound by per mole of base pairs of DNA.
[B]FC_{50} represents the molar concentration of the tested compound that caused a 50% loss of the fluorescence intensity of EB-DNA system.
[C]SC_{50} represents the molar concentration of the tested compound that caused a 50% inhibitory or scavenging effect on $OH^{\bullet}$ or $O_2^{-\bullet}$, its value was calculated from regression line of the log of the tested compound concentration versus the scavenging effect [%] of the compound.

the maximum quenching rate constant of bimolecular diffusion collision, which is indicative of a static type of quenching mechanism arising from the formation of a dark complex between the fluorophore and quenching agent.[23]

Losses of fluorescence intensity at the maximum wavelength may indicate the displacement of EB from EB-DNA complex by a compound and the intercalative binding between the compound with DNA.[15b] Displacement of EB (quantified by fluorescence) by the titration of a compound is suggestive of an intercalative or minor groove binding, thus, EB is particularly suitable as a reporter because of its 24-fold decrease in fluorescence as well as shifts in its excitation spectrum when displaced from an intercalation site.[14b] Fig. S4 shows two representative fluorescence quenching spectra and the corresponding excitation spectra for the fluorescence quenching of EB-DNA systems by the titrations of **2b** and **2c**. Upon increasing amounts of **2b**, the fluorescence emission intensity of the EB-DNA system decreases dramatically with 5 nm blue shifts, simultaneously, the fluorescence excitation intensity of the EB-DNA system decreases dramatically with 7 nm blue shifts at the maximum wavelength by an approximately saturated end point. Similarly, with increasing amounts of **2c**, the dramatic decrease of fluorescence emission intensity with 7 nm red shifts and fluorescence excitation intensity with 9 nm blue shifts takes place. In fact, for all the investigated compounds here, there exist 3–7 nm blue shifts at the maximum wavelength in the fluorescence excitation spectra (data and figures not shown for the other compounds), which indicates that most of the EB molecules can be displaced from EB-DNA complex by every quencher at the saturated end point although 24-fold decreases in fluorescence have not been reached. Thus, it is reasonable that there exists intercalation between DNA and each of the investigated compounds.

Moreover, the Stern–Volmer dynamic quenching constants can also be interpreted as binding affinities of the complex reaction.[24] The data of K_{SV} present the orders of **1b** > **1a** > **1c**, **2b** > **2a** > **2c**, **2a** > **1a**, **2b** > **1b**, and **2c** > **1c**, which indicate the abilities of displacement of EB from EB-DNA systems by compounds and the binding affinities between compounds and DNA. However, it is not in good agreement with the viscosity titration and UV-vis spectroscopy study results. In comparison with the structures of these compounds, for **2a** or **2b**, the phenolic hydroxy group that can binds nucleotides and/or the sugar–phosphate backbone of DNA through hydrogen bond may play a certain role in the EB-DNA quenching tests. Additionally, the other weak interactions such as hydrophobic, van der Waals, and electrostatic forces (pH at 7.20) may not be excluded. In other words, the interaction mechanism is not only determined by complex formation but also by certain weak interactions.[25]

More importantly, DNA intercalators have been used extensively as antitumour, antineoplastic, antimalarial, antibiotic, and antifungal agents.[14a] There is a criterion for screening out antitumour drugs from others by EB-DNA fluorescent tracer method, i.e. a compound can be used as a potential antitumour drug if it causes a 50% loss of fluorescence intensity of EB-DNA by fluorescent titration before the molar concentration ratio of the compound to DNA (nucleotide) does not overrun 100:1.[19] The FC_{50} value is introduced to denote the molar concentration of a compound that causes a 50% loss in the fluorescence intensity of EB-DNA system. According to the data of FC_{50} and the molar ratios of compounds to DNA as shown in Table 3, it is interesting that all the molar concentration ratios of the investigated compounds to DNA are largely under 100:1 at FC_{50}, indicating that all these ligands and Sm^{III} complexes may be used as potential antitumour drugs and the antitumour activities of Sm^{III} complexes are more excellent than those of the ligands. However, their pharmacodynamical and pharmacological properties should be further studied in vivo.

Fluorescence Spectroscopy Study

When excited at $\lambda_{ex} = 321$–325 nm, ligands show the fluorescence maximum wavelengths at $\lambda_{em} = 442$–443 nm, and when excited at $\lambda_{ex} = 321$–323 nm, the Sm^{III} complexes show the fluorescence maximum wavelengths at $\lambda_{em} = 440$–445 nm. Upon addition of DNA, the fluorescence emission intensity of every investigated compound increases steadily. Although the emission enhancement cannot be regarded as a rigid criterion for binding mode, it is related to the extent to which the compound gets into a hydrophobic environment inside DNA and avoids the effect of solvent water molecules. The intrinsic binding constant (K_b) can be obtained by the fluorescence titration and the Scatchard equation.[10,15b] The Scatchard plot should be a straight line for a simple binding reaction. However, the Scatchard plot of r/C_f versus r usually presents a deviation from linearity due to the significant neighbour exclusion properties of DNA binding to intercalating agents.[26] As shown in Fig. S5, the plot of r/C_f versus r for each of the compounds shows a deviation from linearity, so the binding constant was obtained by the McGhee and von Hippel model.[26b,27] The data of binding

parameters are shown in Table 3. It is clear that the data of K_b present the orders of **2a** > **1a**, **2b** > **1b**, and **2c** > **1c**, indicating that the binding of every Sm^{III} complex to DNA is stronger than that of its ligand. The data of K_b present the order of **1b** > **1a** > **1c** and **2b** > **2a** > **2c**, which are consistent with the EB-DNA quenching results. Although it is a weaker binding of **2c** to DNA, **2a** and **2b** are stronger intercalators to DNA in comparison with EB (EB-DNA, $K_b = 3.0 \times 10^6\,M^{-1}$ in 5 mM Tris–HCl/50 mM NaCl buffer, pH 7.2),[28] indicating that the two Sm^{III} complexes can bind to DNA effectively.

Antioxidation Properties

Hydroxyl Radical Scavenging Activity

Figs S6A and B show the plots of hydroxyl radical scavenging effects [%] for ligands and Sm^{III} complexes, respectively, both of them are concentration-dependant. As shown in Table 3, the values of SC_{50} of ligands for $OH^{\bullet}$ are 7.716 ± 0.230–$76.10 \pm 0.372\,\mu M$ with the order of **1b** < **1a** < **1c**, while the values of SC_{50} of Sm^{III} complexes for $OH^{\bullet}$ are 2.127 ± 0.046–$3.792 \pm 0.145\,\mu M$ with the order of **2b** < **2c** < **2a**. It is marked that the scavenging effects of Sm^{III} complexes for $OH^{\bullet}$ are much higher than those of ligands. As for **1b** and its Sm^{III} complex, they show higher abilities of scavenging effects for $OH^{\bullet}$ than other ligands and complexes, possibly due to the key roles of functional groups, –OH, which can react with $OH^{\bullet}$ to form stable macromolecular radicals by the typical H-abstraction reaction.[29] However, there are two types of antioxidation mechanisms for $OH^{\bullet}$, in which one represents suppression of the generation of $OH^{\bullet}$, and another represents the scavenging of $OH^{\bullet}$ generated.[30] The production of $OH^{\bullet}$, detected by ethylene formation from methional, has been investigated in plasma, lymph, and synovial fluid.[30] In the presence of added iron-EDTA as a catalyst, addition of either H_2O_2 or xanthine and xanthine oxidase gives rise to $OH^{\bullet}$ formation that in most cases is not superoxide-dependent. In the absence of the catalyst, the reaction is hardly detectable, the rate being less than 5% of that observed with 1 μM iron-EDTA added. In the present study, it is logical that the chelation between the phenolic hydroxyl group and the carbonyl group of the 2-hydroxybenzoylhydrazine side chain of **1b** with free Fe^{2+} in the iron-EDTA reaction system makes the concentration of free Fe^{2+} much lower so that the catalysis becomes very poor and the $OH^{\bullet}$ formation has been suppressed, therefore, the inhibitive effect of **1b** detected for $OH^{\bullet}$ is higher than other ligands.

Superoxide Radical Scavenging Activity

Figs S6C and D show the plots of superoxide radical scavenging effects [%] for ligands and Sm^{III} complexes, respectively, both of which are also concentration-dependant. As shown in Table 3, the values of SC_{50} of ligands for $O_2^{-\bullet}$ are 4.308 ± 0.174–$6.831 \pm 0.219\,\mu M$ with no significantly different order of **1b** < **1c** < **1a**, but the values of SC_{50} of Sm^{III} complexes for $O_2^{-\bullet}$ are 1.727 ± 0.025–$5.678 \pm 0.153\,\mu M$ with a notably different order of **2c** < **2a** < **2b**. It is clear that the Sm^{III} complex containing *N*-heteroaromatic substituents shows stronger scavenging effects for $O_2^{-\bullet}$. These results suggest that there are different mechanisms between scavenging or inhibiting $OH^{\bullet}$ and $O_2^{-\bullet}$, which should be further studied.

The value of SC_{50} of ascorbic acid (Vc, a standard agent for non-enzymatic reaction) for $OH^{\bullet}$ is $1.537\,mg\,mL^{-1}$ (8.727 mM), and its scavenging effect for $O_2^{-\bullet}$ is only 25% at $1.75\,mg\,mL^{-1}$ (9.94 mM) in vitro.[31] It is pronounced that all the ligands and the Sm^{III} complexes investigated here have much stronger scavenging abilities for $OH^{\bullet}$ and $O_2^{-\bullet}$ than Vc. Considering their oxidative properties, these DNA intercalators may be efficient inhibitors of the formation of a DNA/TBP complex or topoisomerases.

Conclusion

Three Sm^{III} complexes are prepared from $Sm(NO_3)_3 \cdot 6H_2O$ and Schiff-base ligands derived from 8-hydroxyquinoline-2-carboxyaldehyde with three aroylhydrazines including benzoylhydrazine, 2-hydroxybenzoylhydrazine, and isonicotinylhydrazine. Sm^{III} and every ligand can form a dinuclear Sm^{III} complex with a 1:1 metal to ligand stoichiometry and nine-coordination at the Sm^{III} centre. All the ligands and Sm^{III} complexes can strongly bind to CT-DNA through intercalation with the binding constants at 10^5–$10^6\,M^{-1}$. All the ligands and Sm^{III} complexes may be used as potential anticancer drugs but the antitumour activities of Sm^{III} complexes may be more excellent than the ligands. However, their pharmacodynamical and pharmacological properties should be further studied in vivo.

In contrast, all the ligands and Sm^{III} complexes have strong abilities of antioxidation but Sm^{III} complexes present stronger abilities of scavenging $OH^{\bullet}$ than ligands, especially Sm^{III} complex containing active phenolic hydroxy group, while the complex containing *N*-heteroaromatic substituent shows higher scavenging effect for $O_2^{-\bullet}$. There are the similar chemical structures and the similar order of antioxidation and DNA binding properties between Eu^{III} and Sm^{III} complexes. However, the complex $[EuL^2(NO_3)(DMF)_2]_2$ presents a much stronger binding to DNA than $[SmL^2(NO_3)(DMF)_2]_2$ and a reversed order for scavenging $O_2^{-\bullet}$. Considering their oxidative properties, these DNA binders may be effective inhibitors of the formation of a DNA/TBP complex topoisomerases, which should be studied further in vivo. Moreover, the different mechanism between inhibiting or scavenging $OH^{\bullet}$ and $O_2^{-\bullet}$ should be also studied further.

Experimental

Calf thymus DNA (CT-DNA) and ethidium bromide (EB) were obtained from Sigma–Aldrich Biotech. Co., Ltd. 8-Hydroxyquinoline-2-carboxyaldehyde was obtained form J&K Chemical Co., Ltd. The stock solution (1.0 mM) of the investigated compound was prepared by dissolving the powdered material into an appropriate amount of DMF solution. Deionized double distilled water and analytical grade reagents were used throughout. CT-DNA stock solution was prepared by dissolving the solid material, normally at $0.3\,mg\,mL^{-1}$, in 5 mM Tris–HCl buffer (pH 7.20) containing 50 mM NaCl. Then, the solution was kept over 48 h at 4°C. The resulting somewhat viscous solution was clear and particle-free. The solution of CT-DNA in Tris–HCl buffer gave a ratio of UV-vis absorbance at 260 to 280 nm of ~1.8–1.9:1, indicating that the CT-DNA was sufficiently free of protein. The CT-DNA concentration in terms of base pair L^{-1} was determined spectrophotometrically by employing an extinction coefficient of $\varepsilon_{max} = 13200\,M^{-1}\,cm^{-1}$ (base pair)$^{-1}$ at 260 nm, while the concentration in terms of nucleotide L^{-1} was determined by employing an extinction coefficient of $6600\,M^{-1}\,cm^{-1}$ (nucleotide)$^{-1}$ at 260 nm.[32] The CT-DNA stock solution was stored at –20°C until it was used. A working standard solution of CT-DNA was obtained by appropriate dilution of the stock solution in 5 mM Tris–HCl buffer (pH 7.20) containing 50 mM NaCl. EB was dissolved in 5 mM

Tris–HCl buffer (pH 7.20) and its concentration was determined assuming a molar extinction coefficient of 5600 M^{-1} cm^{-1} at 480 nm.[14a]

The melting points of the compounds were determined on an XT4–100X microscopic melting point apparatus (Beijing, China). Elemental analyses of C, N, and H were carried out on an Elemental Vario EL analyzer. The Sm^{III} content was determined by complexo-metric titration with EDTA after destruction of the complex in the conventional manner. ^1H NMR spectra were recorded on a Bruker Avance DRX 200 MHz spectrometer (DMSO-d_6) with TMS as an internal standard. The IR spectra were recorded on a Nicolet Nexus 670 FT-IR spectrometer using KBr disc in the 4000–400 cm^{-1} region. ESI-MS (ESI-Trap/Mass) spectra were recorded on a Bruker esquire 6000 mass spectrophotometer.

Viscosity titration experiments were carried on an Ubbelodhe viscometer in a thermostated water-bath maintained at 25.00 ± 0.01°C. Titrations were performed for an investigated compound that was introduced into DNA solution (50 μM, bps) present in the viscometer. Data were presented as $(\eta/\eta_o)^{1/3}$ versus the ratio of the compound to DNA, where η is the viscosity of DNA in the presence of the compound corrected from the solvent effect, and η_o is the viscosity of DNA alone. Relative viscosities for DNA in either the presence or absence of compound were calculated from the following relation:

$$\eta = (t - t_o)/t_o, \quad (1)$$

where t is the observed flow time of the DNA containing solution, and t_o is the flow time of buffer.[14a,15a]

UV-vis spectra were obtained using a Perkin–Elmer Lambda UV-vis spectrophotometer. The UV-vis absorption spectra of the investigated compounds in the absence and in the presence of the CT-DNA were obtained in 1:100 solution of DMF: Tris–HCl buffer (5 mM, pH 7.20) containing 50 mM NaCl, respectively.

Fluorescence spectra were recorded using RF–5301PC spectrofluorophotometer (Shimadzu, Japan) with a 1 cm quartz cell. All the experiments were measured after 5 min at constant room temperature, 298 K. The intrinsic binding constant K_b was obtained by the fluorescence titration and the McGhee and von Hippel model:[10,26b,27]

$$\frac{r}{C_f} = K_b(1 - nr)\left[\frac{1 - nr}{1 - (n - 1)r}\right]^{n-1}, \quad (2)$$

where r is the moles of compound bound per mole nucleotides of DNA; C_f is the molar concentration of free compound; K_b is the intrinsic binding constant; n is the exclusion parameter in DNA base pairs, while the data of $1/n$ represent moles of the tested compound bound by per mole of base pairs of DNA. C_f and r were calculated according to the following equations:

$$C_f = C_t - C_b \quad (3)$$

$$C_b = C_t(F - F_o)/(F_{max} - F_o) \quad (4)$$

$$r = C_b/C_{DNA}, \quad (5)$$

where C_t is the total molar concentration of compound; C_b is the molar concentration of compound bound for DNA; F is the observed fluorescence emission intensity at a given DNA concentration C_{DNA} (nucleotide); F_o is the fluorescence emission intensity in the absence of DNA; F_{max} is the maximum fluorescence emission intensity of the compound totally bound for DNA at a titration end point. The experimental parameters K_b and n were adjusted to produce curves that gave, by inspection, the most satisfactory fits to the experimental data.

The EB-DNA quenching assay was performed as reported in a literature but a slight amendment.[10,33] DNA (2.0 μM, bps) solution was added incrementally to 0.32 μM EB solution, until the rise in the fluorescence ($\lambda_{ex} = 496$ nm, $\lambda_{em} = 596$ nm) attained a saturation. Then, small aliquots of concentrated compound solutions (1.0 mM) were added until the drop in fluorescence intensity ($\lambda_{ex} = 525$ nm, $\lambda_{em} = 587$ nm) reached a constant value. The experiments were measured after 5 min at a constant room temperature, 298 K. The Stern–Volmer equation was used to determine the fluorescent quenching mechanism:[14a]

$$F_o/F = 1 + K_q\tau_o[Q] = 1 + K_{SV}[Q], \quad (6)$$

where F_o and F are the fluorescence intensity in the absence and in the presence of a compound at $[Q]$ concentration, respectively; K_{SV} is the Stern–Volmer dynamic quenching constant; K_q is the quenching rate constant of bimolecular diffusion collision; τ_o is the fluorescent lifetime of EB-DNA.

The hydroxyl radicals in aqueous media were generated through the Fenton-type reaction.[30,34] The 5-mL reaction mixtures contained 2.0 mL of 100 mM phosphate buffer (pH = 7.4), 1.0 mL of 0.10 mM aqueous safranin, 1 mL of 1.0 mM aqueous EDTA–Fe^{II}, 1 mL of 3% aqueous H_2O_2, and a series of quantitatively micro-adding solution of the tested compound. The sample without the tested compound was used as the control. The reaction mixtures were incubated at 37°C for 60 min in a water-bath. The absorbance at 520 nm was measured and the solvent effect was corrected throughout. The scavenging effect for $OH^\bullet$ was calculated from the following expression:[15b,35]

$$\text{Scavenging effect } [\%] = \frac{A_{sample} - A_{blank}}{A_{control} - A_{blank}} \times 100, \quad (7)$$

where A_{sample} is the absorbance of the sample in the presence of the tested compound, A_{blank} is the absorbance of the blank in the absence of the tested compound, and $A_{control}$ is the absorbance in the absence of the tested compound and EDTA–Fe^{II}.

The superoxide radicals ($O_2^{-\bullet}$) were produced by the MET–$VitB_2$–NBT system.[15b,35] The solution of MET (methionine), $VitB_2$ (vitamin B2), and NBT (nitroblue tetrazolium) were prepared with deionized double distilled water and avoiding light. The 5-mL reaction mixtures contained 2.5 mL of 100 mM phosphate buffer (pH 7.8), 1.0 mL of 50 mM MET, 1.0 mL of 0.23 mM NBT, 0.50 mL of 33 μM $VitB_2$, and a series of quantitatively microadding solution of the tested compound. After incubation at 30°C for 10 min in a water bath and then illuminated with a fluorescent lamp (4000 Lux), the absorbance of the sample was measured at 560 nm and the solvent effect was corrected throughout. The sample reaction mixtures without the tested compound were used as the control. The scavenging effect for $O_2^{-\bullet}$ was calculated from the following expression:

$$\text{Scavenging effect } [\%] = \frac{A_o - A_i}{A_o} \times 100, \quad (8)$$

where A_i is the absorbance in the presence of the tested compound and A_o is the absorbance in the absence of the tested

compound. The data for antioxidation presented as means ± s.d. of three determinations and followed by Student's *t*-test. Differences were considered to be statistically significant if $P < 0.05$. The SC_{50} value was introduced to denote the molar concentration of the tested compound, which caused a 50% scavenging effect on $OH^{\bullet}$ or $O_2^{-\bullet}$.

Preparation of Ligands and Complexes

Ligands **1a**–**c** were prepared using a previously described literature method.[10] Complex **2a** was prepared by refluxing and stirring equimolar amounts of a 40-mL methanol solution of **1a** (0.058 g, 0.2 mmol) and $Sm(NO_3)_3 \cdot 6H_2O$ on a water-bath. After refluxing for 30 min, triethylamine (0.020 g, 0.2 mmol) was added into the reaction mixtures dropwise to deprotonate the phenolic hydroxyl substituent of the 8-hydroxyquinolinato unit. Then, the mixtures were refluxed and stirred continuously for 8 h. After cooling to room temperature, the precipitate was centrifuged, washed with methanol, and dried in vacuum over 48 h to give an orange powder. Yield 87.0% (0.094 g). *m/z* (ESI-MS) 1297.1 $[M+H]^+$, 648.2 $[M/2+H]^+$ (DMF solution). Λm (DMF) 37.3 $cm^2\,\Omega^{-1}\,mol^{-1}$. Anal. Calc. for $C_{34}H_{30}N_8O_{14}Sm_2$ (1075.8): C 37.93, H 2.79, N 10.41, Sm 27.96. Found. C 38.03, H 2.79, N 10.38, Sm 27.91%.

Complex **2b** was prepared from equimolar amounts of $Sm(NO_3) \cdot 6H_2O$ and **2b** as the method of **2a**. Yield 90.2%. *m/z* (ESI-MS) 1329.2 $[M+H]^+$, 665.4 $[M/2+H]^+$ (DMF solution). Λm (DMF) 38.8 $cm^2\,\Omega^{-1}\,mol^{-1}$. Anal. Calc. for $C_{34}H_{30}N_8O_{16}Sm_2$ (1107.8): C 36.83, H 2.71, N 10.11, Sm 27.15. Found. C 36.80, H 2.70, N 10.08, Sm 27.22%.

Complex **2c** was prepared from equimolar amounts of $Sm(NO_3) \cdot 6H_2O$ and **1c** as the method of **2a**. Yield 88.3%. *m/z* (ESI-MS) 1299.2 $[M+H]^+$, 649.2 $[M/2+H]^+$ (DMF solution). Λm (DMF) 30.1 $cm^2\,\Omega^{-1}\,mol^{-1}$. Anal. Calc. for $C_{32}H_{28}N_{10}O_{14}Sm_2$ (1077.8): C 35.63, H 2.60, N 12.99, Sm 27.91. Found. C 35.60, H 2.61, N 13.03, Sm 27.85.

Determination of Crystal Structures

The radiation used for a crystal was graphite-monochromated Mo Kα radiation (0.71073 Å) and the data were collected on a Bruker APEX area-detector diffractometer by the ω–2θ scan technique at 298(2) K. The structures were solved by direct methods. All non-hydrogen atoms were refined anisotropically by full-matrix least-squares methods on F^2. Primary non-hydrogen atoms were found from direct methods and secondary non-hydrogen atoms were found from difference maps. The hydrogen atoms were added geometrically and their positions and thermal vibration factors were constrained. All calculations were performed using the programs *SHELXS-97* and *SHELXL-97*.[36]

Accessory Publication

Supporting information containing the crystal data, UV-vis spectra values, characteristic IR band data, McGhee and von Hippel plots and plots of antioxidation properties for the investigated compounds are available from the Journal's website. CCDC 704943 (**2a′**), 704944 (**2b′**), and 704945 (**2c′**) contain the supplementary crystallographic data for this paper. These data can be obtained free of charge from The Cambridge Crystallographic Data Centre via www.ccdc.cam.ac.uk/data_request/cif.

Acknowledgement

This study was supported by the National Natural Science Foundation of China (20975046) and Gansu CSRPS (1010B-04).

References

[1] (a) L. H. Schmidt, *Annu. Rev. Microbiol.* **1969**, *23*, 427. doi:10.1146/ANNUREV.MI.23.100169.002235
(b) A. A. El-Asmy, A. Z. El-Sonbati, A. A. Ba-Issa, M. Mounir, *Transition Met. Chem.* **1990**, *15*, 222. doi:10.1007/BF01038379

[2] (a) D. Parker, R. S. Dickins, H. Puschmann, C. Crossland, J. A. K. Howard, *Chem. Rev.* **2002**, *102*, 1977. doi:10.1021/CR010452+
(b) M. Albrecht, O. Osetska, R. Fröhliich, *Dalton Trans.* **2005**, *23*, 3757. doi:10.1039/B507621H
(c) R. B. Hunter, W. Walker, *Nature* **1956**, *178*, 47. doi:10.1038/178047A0
(d) D. M. Kramsch, A. J. Aspen, L. J. Rozler, *Science* **1981**, *213*, 1511. doi:10.1126/SCIENCE.6792706

[3] (a) E. M. Hodnett, P. D. Mooney, *J. Med. Chem.* **1970**, *13*, 786. doi:10.1021/JM00298A065
(b) E. M. Hodnett, W. J. Dunn, *J. Med. Chem.* **1972**, *15*, 339. doi:10.1021/JM00273A037

[4] (a) Y. B. Zeng, N. Yang, W. S. Liu, N. Tang, *J. Inorg. Biochem.* **2003**, *97*, 258. doi:10.1016/S0162-0134(03)00313-1
(b) A. M. Pyle, T. Morii, J. K. Barton, *J. Am. Chem. Soc.* **1990**, *112*, 9432. doi:10.1021/JA00181A077
(c) J. K. Barton, J. M. Goldberg, C. V. Kumar, N. J. Turro, *J. Am. Chem. Soc.* **1986**, *108*, 2081. doi:10.1021/JA00268A057

[5] (a) S. Mahadevan, M. Palaniandavar, *Inorg. Chim. Acre* **1997**, *254*, 291. doi:10.1016/S0020-1693(96)05175-4
(b) S. J. Lippard, *Acc. Chem. Res.* **1978**, *11*, 211. doi:10.1021/AR50125A006
(c) S. M. Hecht, *Acc. Chem. Res.* **1986**, *19*, 383. doi:10.1021/AR00132A002

[6] (a) N. Grover, N. Gupta, H. H. Thorp, *J. Am. Chem. Soc.* **1992**, *114*, 3390. doi:10.1021/JA00035A034
(b) L. J. Govenlock, C. E. Mathieu, C. L. Maupin, D. Parker, J. P. Riehl, G. Siligardi, J. A. G. Williams, *Chem. Commun.* **1999**, *17*, 1699. doi:10.1039/A904257A

[7] (a) B. N. Ames, M. K. Shigenaga, T. M. Hagen, *Proc. Natl. Acad. Sci. USA* **1993**, *90*, 7915. doi:10.1073/PNAS.90.17.7915
(b) A. A. Horton, S. Fairhurst, *Crit. Rev. Toxicol.* **1987**, *18*, 27. doi:10.3109/10408448709089856
(c) H. L. Wang, Z. Y. Yang, B. D. Wang, *Transition Met. Chem.* **2006**, *31*, 470. doi:10.1007/S11243-006-0015-3

[8] S. F. Lo, V. Mulabagal, C. L. Chen, C. L. Kuo, H. S. Tsay, *J. Agric. Food Chem.* **2004**, *52*, 6916. doi:10.1021/JF040017R

[9] (a) S. Y. Chiang, J. Welch, F. J. Rauscher, T. A. Beerman, *Biochemistry* **1994**, *33*, 7033. doi:10.1021/BI00189A003
(b) J. M. Woynarowski, M. Mchugh, R. D. Sigmund, T. A. Beerman, *Mol. Pharmacol.* **1989**, *35*, 177.
(c) A. Y. Chen, C. Yu, B. Gatto, L. F. Liu, *Proc. Natl. Acad. Sci. USA* **1993**, *90*, 8131. doi:10.1073/PNAS.90.17.8131

[10] Y. C. Liu, Z. Y. Yang, *J. Inorg. Biochem.* **2009**, *103*, 1014. doi:10.1016/J.JINORGBIO.2009.04.013

[11] W. J. Geary, *Coord. Chem. Rev.* **1971**, *7*, 81. doi:10.1016/S0010-8545(00)80009-0

[12] (a) M. M. Moawad, W. G. Hanna, *J. Coord. Chem.* **2002**, *55*, 439. doi:10.1080/00958970211906
(b) T. M. A. Ismail, *J. Coord. Chem.* **2005**, *58*, 141. doi:10.1080/0095897042000274733

[13] J. M. Ou-Yang, *J. Inorg. Chem* **1997**, *13*, 315 (in Chinese).

[14] (a) D. Suh, J. B. Chaires, *Bioorg. Med. Chem.* **1995**, *3*, 723. doi:10.1016/0968-0896(95)00053-J
(b) R. Palchaudhuri, P. J. Hergenrother, *Curr. Opin. Biotechnol.* **2007**, *18*, 497. doi:10.1016/J.COPBIO.2007.09.006

[15] (a) S. Satyanarayana, J. C. Dabrowiak, J. B. Chaires, *Biochemistry* **1992**, *31*, 9319. doi:10.1021/BI00154A001

(b) B. D. Wang, Z. Y. Yang, P. Crewdson, D. Q. Wang, *J. Inorg. Biochem.* **2007**, *101*, 1492. doi:10.1016/J.JINORGBIO.2007.04.007

[16] R. D. Snyder, *Mutat. Res.* **2007**, *623*, 72. doi:10.1016/J.MRFMMM.2007.03.006

[17] (a) J. K. Barton, A. T. Danishefsky, J. M. Goldberg, *J. Am. Chem. Soc.* **1984**, *106*, 2172. doi:10.1021/JA00319A043
(b) H. L. Lu, J. J. Liang, Z. Z. Zeng, P. X. Xi, X. H. Liu, F. J. Chen, Z. H. Xu, *Transition Met. Chem.* **2007**, *32*, 564. doi:10.1007/S11243-007-0202-X

[18] (a) V. G. Vaidyanathan, B. U. Nair, *Eur. J. Inorg. Chem.* **2004**, 1840. doi:10.1002/EJIC.200300718
(b) P. X. Xi, Z. H. Xu, X. H. Liu, F. J. Chen, L. Huang, Z. Z. Zeng, *Chem. Pharm. Bull.* **2008**, *56*, 541. doi:10.1248/CPB.56.541

[19] Z. L. Li, J. H. Chen, K. C. Zhang, M. L. Li, R. Q. Yu, *Sci. China Series B. Chem.* **1991**, *11*, 1193 (in Chinese).

[20] (a) C. Behrens, N. Harrit, P. E. Nielsen, *Bioconjug. Chem.* **2001**, *12*, 1021. doi:10.1021/BC0100556
(b) S. Frau, J. Bernadou, B. Meunier, *Bioconjug. Chem.* **1997**, *8*, 222. doi:10.1021/BC970007E

[21] (a) D. S. Sigman, A. Mazumder, D. M. Perrin, *Chem. Rev.* **1993**, *93*, 2295. doi:10.1021/CR00022A011
(b) Y. Wang, Z. Y. Yang, Q. Wang, Q. K. Cai, K. B. Yu, *J. Organomet. Chem.* **2005**, *690*, 4557. doi:10.1016/J.JORGANCHEM.2005.07.046

[22] J. Z. Wu, B. H. Ye, L. Wang, L. N. Ji, J. Y. Zhou, R. H. Li, Z. Y. Zhou, *J. Chem. Soc., Dalton Trans.* **1997**, *8*, 1395. doi:10.1039/A605269J

[23] (a) Y. C. Liu, Z. Y. Yang, J. Du, X. J. Yao, R. X. Lei, X. D. Zheng, J. N. Liu, H. S. Hu, H. Li, *Chem. Pharm. Bull.* **2008**, *56*, 443. doi:10.1248/CPB.56.443
(b) Y. C. Liu, Z. Y. Yang, J. Du, X. J. Yao, R. X. Lei, X. D. Zheng, J. N. Liu, H. S. Hu, H. Li, *Immunobiology* **2008**, *213*, 651. doi:10.1016/J.IMBIO.2008.02.003

[24] (a) L. A. Bagatolli, S. C. Kivatinitz, G. D. Fidelio, *J. Pharm. Sci.* **1996**, *85*, 1131. doi:10.1021/JS960142K
(b) M. M. Yang, P. Yang, L. W. Zhang, *Chin. Sci. Bull.* **1994**, *9*, 31.

[25] A. Ayar, B. Mercimek, *Process Biochem.* **2006**, *41*, 1553. doi:10.1016/J.PROCBIO.2006.02.016

[26] (a) L. M. Berezhkovskiy, I. V. Astafieva, C. Cardoso, *Anal. Biochem.* **2002**, *308*, 239. doi:10.1016/S0003-2697(02)00211-7
(b) J. B. Chaires, N. Dattagupta, D. M. Crothers, *Biochemistry* **1982**, *21*, 3933. doi:10.1021/BI00260A005

[27] J. D. McGhee, P. H. von Hippel, *J. Mol. Biol.* **1974**, *86*, 469. doi:10.1016/0022-2836(74)90031-X

[28] (a) M. Baldini, M. Belicchi-Ferrari, F. Bisceglie, G. Pelosi, S. Pinelli, P. Tarasconi, *Inorg. Chem.* **2003**, *42*, 2049. doi:10.1021/IC026131D
(b) Y. Wang, Z. Y. Yang, Z. N. Chen, *Bioorg. Med. Chem. Lett.* **2008**, *18*, 298. doi:10.1016/J.BMCL.2007.10.085

[29] J. I. Ueda, N. Saito, Y. Shimazu, T. Ozawa, *Arch. Biochem. Biophys.* **1996**, *333*, 377. doi:10.1006/ABBI.1996.0404

[30] C. C. Winterbourn, *Biochem. J.* **1981**, *198*, 125.

[31] R. Xing, H. Yu, S. Liu, W. Zhang, Q. Zhang, Z. Li, P. Li, *Bioorg. Med. Chem.* **2005**, *13*, 1387. doi:10.1016/J.BMC.2004.11.002

[32] F. Zsila, Z. Bikádi, M. Simonyi, *Org. Biomol. Chem.* **2004**, *2*, 2902. doi:10.1039/B409724F

[33] A. G. Krishna, D. V. Kumar, B. M. Khan, S. K. Rawal, K. N. Ganesh, *Biochim. Biophys. Acta* **1998**, *1381*, 104.

[34] C. C. Winterbourn, *Biochem. J.* **1979**, *182*, 625.

[35] Z. Y. Guo, R. Xing, S. Liu, H. H. Yu, P. B. Wang, C. P. Li, P. C. Li, *Bioorg. Med. Chem. Lett.* **2005**, *15*, 4600. doi:10.1016/J.BMCL.2005.06.095

[36] G. M. Sheldrick, *Acta Crystallogr. A* **1990**, *46*, 467. doi:10.1107/S0108767390000277